Journal of Zhejiang University-SCIENCE A (Applied Physics & Engineering) 2025 26(1):78-86
www.jzus.zju.edu.cn; www.springer.com/journal/11582
E-mail: jzus_a@zju.edu.cn

Research Articles

https://doi.org/10.1631/jzus.A2300398

Design and experimental validation of an electromagnetic launching mechanism for a tethered net

Zongming ZHU, Weihao LUO, Zongjing LIN, Yuzhe KANG, Maoying ZHOU✉, Ban WANG✉, Huawei QIN

School of Mechanical Engineering, Hangzhou Dianzi University, Hangzhou 310018, China

Abstract: High-altitude rescue is dangerous and difficult. A new rescue method is proposed here based on electromagnetically launched tethered nets. Four electromagnetic launching units are attached to a revolving platform, from which four projectiles are launched. The four projectiles are connected to a tethered net, bringing it into motion. As the tethered net approaches and comes into contact with the object, the object will be trapped, and the rescue task will then be completed as long as the tethered net can be restored along with the trapped object. The structural design of the electromagnetic launching unit is presented with the established mathematical model. The motion characteristics of the launched projectiles are studied and their exit velocities are modeled and measured. Terminal velocities of these projectiles are characterized, and the final shape and position of the projected tethered net are obtained. This study validates the feasibility of using electromagnetically launched tethered nets to perform high-altitude rescues.

Key words: Electromagnetic launching; Tethered-net launching; High-altitude rescue; Trajectory

1 Introduction

With the increasing number of tall buildings in cities, high-altitude accidents have become an essential concern for the public. Yet, high-altitude rescues are extremely difficult. On one hand, people involved in these accidents are usually so nervous that they cannot respond well to rescuers. On the other hand, the available types of rescuing equipment are limited and consequently, the help and support provided for the rescued are insufficient. Indeed, in such situations, manual rescue is the only choice, with psychological interventions adopted to ease the stress of the rescued. In addition, air cushions are deployed for final protection for the rescued and the rescuer (Faraj et al., 2022). This rescue process is inherently inefficient and ineffective. Psychological interventions require professional psychological counselors, who are not widely accessible. Manual rescue is simple but poses high requirements for the rescuer. Sometimes the rescuers are even put in danger in the process of rescuing. A passive air cushion is commonly used but cumbersome and generally hard to move, limiting its protective capability, and its deployment is also time-consuming. Thus, there are many problems with existing high-altitude rescue methods. To this end, we investigated the possibility of flexible capturing and recovering technology for objects with high safety and good fault tolerance.

Recently, tethered nets have been given special attention due to their ability to capture or trap objects. Successful applications include the clean-up of space debris (Chen et al., 2009) and the capture of low-altitude drones (Chen et al., 2022). A key concern for tethered-net object-trapping systems is the launching or shooting of the tethered net. Many investigations have been conducted with various launching methods proposed and tested, including gunpowder, compressed gas, compression springs, and electromagnetic motors. Liu et al. (2022) used gunpowder to launch mass blocks. First, electric signals were used to control gunpowder initiation. During the ignition process, the internal energy of the gunpowder was continuously transformed into the kinetic energy of the mass blocks, and the net was successfully launched after the mass blocks flew out. This kind of launching technology is

✉ Maoying ZHOU, myzhou@hdu.edu.cn
Ban WANG, bigban@zju.edu.cn
Maoying ZHOU, https://orcid.org/0000-0002-0306-7863

Received Aug. 4, 2023; Revision accepted Jan. 8, 2024;
Crosschecked Oct. 21, 2024; Online first Dec. 7, 2024

very mature, but the launch efficiency is low, and the environmental pollution caused is serious. Yu et al. (2022) used compressed gas to launch mass blocks. The gas in the tank was released through an air valve, and the mass block was launched using the energy generated instantaneously by the compressed gas. This method is relatively simple in principle and easy to implement, but it requires a gas tank and air valves. European Space Agency (ESA) launched mass blocks by compressing springs in the project of Robotic Geostationary Orbit Restorer (Bischof, 2003). The spring was compressed before launching, and the elastic potential energy was converted into the kinetic energy of the mass blocks during spring release. This launching method is also simple and easy to implement, but it is difficult to accurately control the launching velocity of the mass blocks. Sinn et al. (2013) used the kinetic energy generated by the rotation of an electromagnetic motor to launch mass blocks. When the motor rotated, the mass blocks were successfully launched through the action of centrifugal force. This launching mode is suitable for the spinning deployment mode of a net. Through the analysis of these traditional launching methods, we found that they all present problems in the task of tethered-net launching. On the other hand, electromagnetic launching has been extensively utilized and studied in military and aeronautical applications (Fair, 2009; Ma et al., 2019). With the help of electromagnetic forces, a projectile can be accelerated to a high speed in a short time with high energy efficiency. Further, depending on the working principles and detailed structures, electromagnetic launching devices fall into three categories: rail launchers (McNab, 2003), coil launchers (Kaye, 2004), and reconnection launchers (Brown et al., 2002). Three types of electromagnetic launching devices are shown in Fig. S8 of the electronic supplementary materials (ESM).

A rail launcher usually consists of two placed metal rails, one sliding armature spanning the two rails, and an external pulsed power supply. Under the pulsed power, the sliding armature assumes a pulsed current and accelerates under the action of Lorentz force (Nechitailo and Lewis, 2006). This sort of launcher has a simple structure. However, contact between the rails and the armature must be maintained during the launching process, leading to serious structural ablation and wear (Meinel, 2007). As a result, the service life is very short and launching efficiency is low.

Coil launchers are mainly comprised of a cylindrical driving coil, power supply, and projectile (Barnes et al., 2004). Based on the main driving force of the projectile inside the coil, the coil launcher can be either an inductance coil launcher or a reluctance coil launcher (Slade, 2005; Su et al., 2015). In an inductance coil launcher, a hollow metal projectile is typically used. When the driving coil is supplied with electrical voltage, current loops form in the coil and an electromagnetic field is induced around it. Eddy current is induced in the projectile, which is driven through the coil under the action of electromagnetic force, or inductive thrust. In comparison, a reluctance coil launcher utilizes a solid cylindrical ferromagnetic projectile. Thrust for the projectile mainly comes from magnetic attraction from the generated magnetic field in the coil, or the magnetized thrust. Indeed, inductive thrust and magnetized thrust are in opposite directions. The magnetized thrust pulls the projectile from the exit to the center of the solenoid, while the inductive thrust pushes the projectile from the center to the exit of the solenoid (Orbach et al., 2022).

Finally, a reconnection launcher consists of multiple tandem driving coils and a planar moving armature (Cowan et al., 1986). In essence, the reconnection launcher is a special type of inductance coil launcher. What makes it different is the number of driving coils involved and the orientation of the established magnetic field. There is no direct contact between the moving armature and the driving coil. Hence, the launching efficiency is higher than that of a rail launcher. However, this technology is relatively immature due to its structural complexity. After comparing these electromagnetic launching devices, we decided that a coil launcher would be most appropriate for small-scale applications due to its simple structure and fabrication and the ease of control and actuation.

In this study, we focused on the electromagnetic launching of a tethered net using a coil launcher. The driving circuits of the coil-launching units were designed with zero-voltage-switch (ZVS) booster modules. We theoretically modeled the exit velocity of the projectile, and investigated it experimentally. We evaluated the launched tethered net along with the connected projectiles in terms of their flight in the air. A simple experiment was then conducted to validate the capturing capability of the tethered net.

2 Design of the tethered-net launcher

Reluctance coil-launching units were adopted here in the establishment of an electromagnetically launched tethered net, as shown in Fig. 1. The launching unit was composed of mechanical and electrical parts. The mechanical parts included a solid-cylinder ferromagnetic projectile, a long cylindrical tube to guide the projectile, and a driving coil wound on the outer surface of the cylindrical tube. The electrical part consisted of a capacitor for electrical storage, a ZVS booster module, two circuit switches, a freewheel diode, a silicon-controlled rectifier (SCR), and a 12 V battery pack as the power supply.

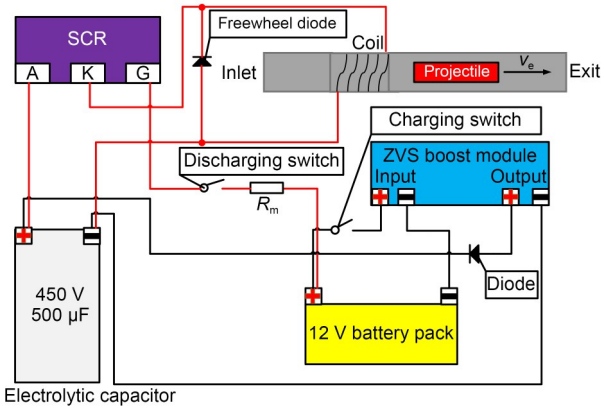

Fig. 1 Schematic diagram of the reluctance-coil launcher. R_m is the current-limiting resistance; v_e is the exit velocity

The working process of the reluctance coil-launching unit can be divided into two stages. In the first stage, the charging switch is flipped on and the coil wound upon the cylindrical tube is disconnected from the capacitor. This is achieved with the help of the SCR (70TPS16) in an OFF state. As a result, the electrical part works in a charging mode. Direct-current (DC) voltage output from the battery is fed into the ZVS booster module and converted into a high-voltage DC output. This high voltage is used to charge the electrolytic capacitor (450 V, 500 μF). In the second stage, the projectile is prepared to be launched. When the capacitor is charged to the desired voltage, the projectile is launched. The discharging switch is flipped on and the charging switch is simultaneously flipped off. The SCR is in an ON state to enable the connection of the coil to the capacitor. The resulting current in the coil leads to a magnetic field inside the tube, which magnetizes the ferromagnetic projectile and pulls it from the entrance to the center position of the coil. In this course, the projectile is in the acceleration phase. When the projectile moves beyond the center of the coil, the magnetic forces exerted upon the projectile act as drag and try to pull it back. The projectile then enters the deceleration phase. In this design, a freewheel diode (Fr607) is connected in parallel with the coil to protect the SCR from possible breakdown due to high voltage.

With the help of reluctance coil-launching units, the tethered-net launcher was established as shown in Fig. 2a. The launcher was composed of a base plate, four reluctance-coil-launching units, a pitching platform, a launching-adjustment mechanism, and a tethered-net storage. The launching angle α was between the axis of the launching unit and the central axis of the tethered-net storage, while the pitching angle β was used to make the coil at the bottom of the launching units parallel to the horizontal plane, as shown in Fig. 2b. In addition, the launching angle α was adjustable mainly by connecting different through-holes with bolts and nuts, as shown in Fig. 2c. The tethered-net storage and the four reluctance-coil-launching units were fixed to the base plate, with the tethered-net storage located in the center and the four reluctance-coil-launching units located in a circular array. Four projectiles are launched from the corresponding coil-launching units directly connected to the tethered net. Initially, the tethered net is kept in the tether-net storage. When the four projectiles are launched, they will move in the air and pull the tethered net forward until they fall onto the ground or come into contact with the object. Four capacitors were used to power the four coil launchers, connected in parallel. To prevent interference between different capacitors, four high-voltage diodes (6A10) were placed in the circuits.

3 Theoretical model of the tethered-net launcher

3.1 Reluctance coil-launching unit

With regard to the reluctance coil-launching unit, the magnetization of the ferromagnetic projectile leads to the formation of a magnetic circuit between the coil and the projectile. According to the reluctance principle, the magnetic flux always tends to flow through the path with minimum reluctance (Bresie and Andrews, 1991). Therefore, the reluctance between

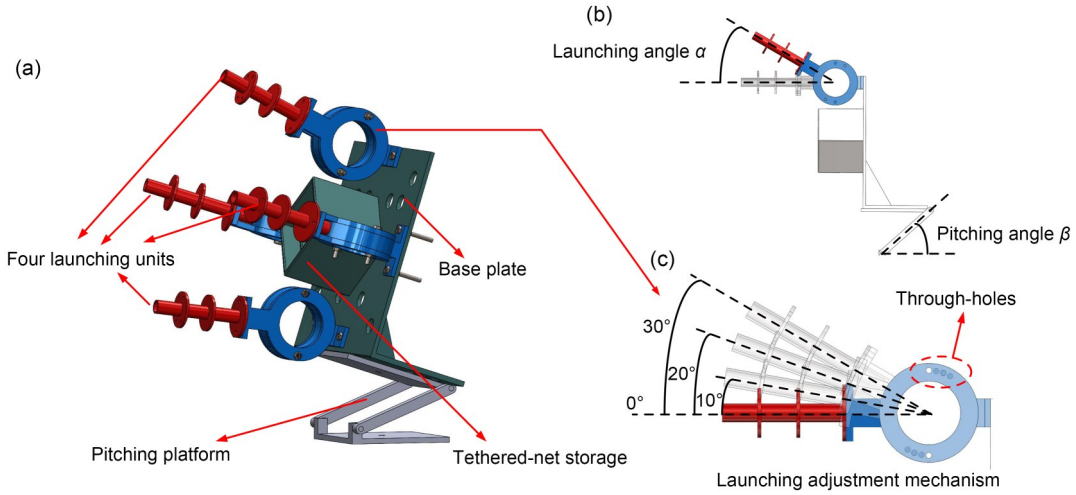

Fig. 2 Schematic diagram of the structure and principle of the tethered-net launcher: (a) schematic diagram of the tethered-net launcher; (b) description of the launching angle and pitching angle; (c) principle of the launching adjustment mechanism

the coil and the projectile is varied, and the projectile always tries to get aligned in the minimum reluctance axis. In this sense, we can approximately express the exit velocity v_e as:

$$v_e = \sqrt{\frac{C}{m}U_p^2 - \frac{2W_{fric}}{m}}, \quad (1)$$

where U_p and C are the initial charged voltage and capacitance of the capacitor, respectively, W_{fric} is the work done by frictional forces in the process of launching, and m is the mass of the projectile. The derivation of Eq. (1) is detailed in Section S1 of the ESM.

It can be seen from Eq. (1) that the square of the charged voltage of the capacitor is linearly related to the square of the exit velocity of the projectile.

3.2 Motion of the projectile and the tethered net

The dynamics of the projectile are rather complex and should be divided into several stages. Inside the coil launcher, its dynamics are subject to the magnetic force, air drag, gravity, and frictional forces. Immediately after launching and before contacting the objects, the projectile flies in the air under the action of gravity, air drag F_{drag}, and tension $F_{tension}$ from the connecting thread. After contacting objects, the projectile dynamics couple strongly with the captured objects.

Neglecting the reactive tension $F_{tension}$, the motion of one projectile can be sketched in a two-dimensional way. Indeed, as the gravity force is always in the vertical direction towards the earth, and the air drag F_{drag} is always in the opposite direction of the current velocity vector, the y axis can be chosen as the opposite direction to gravity, and the x axis can be chosen as perpendicular to the y axis and pointing in the moving direction of the projectile. The kinematics modeling process for the projectile is given in Section S2 of the ESM.

4 Experiments and discussion

4.1 Exit velocity of the projectile

The first concern is the launching performance of the coil-launching unit, on which the exit velocity v_e is focused. The geometrical structure of the designed reluctance coil-launching unit and the measuring system are given in Section S3 of the ESM.

Different diameters of wire for the coil were selected (0.4 mm, 0.6 mm, 0.8 mm, and 1.0 mm). The four groups of coils adopted in the prototypes of the coil-launching units are given in Table S1 of the ESM. With the total length of the coil fixed, the number of turns in the coil, as well as the final resistance and inductance of the fabricated coils, was obtained with the help of a digital multimeter. In addition, the actual capacitance value of the capacitor was measured as 457 μF.

With the above-mentioned measuring system, we measured the exit velocity of the projectile for different groups of coils with different charged voltages for

the capacitors. With the help of Eq. (1), the functional relations between v_e and U_p were fitted using linear regression. The results are shown in Fig. S9 of the ESM. A direct comparison between the measured and fitted results showed that the established model for the exit velocity is valid and can be used for future design and optimization.

4.2 Current in the coils during launching

The mechanical part of the launching prototype is shown in Fig. 3a. To facilitate subsequent experiments, the coils were numbered counterclockwise as 1, 2, 3, and 4. The electrical part shown in Fig. 3b was used to control the launch of the tethered net.

Due to the limited outer diameter of coil baffles on the launching tube, for better launching performance, we determined that the wire diameter of the coils used in the tethered-net launcher should be 0.6 mm, and the number of turns in the coils should be set to 420. The parameters of the four coils are given in Table S2 of the ESM. With the established prototype of the tethered-net launcher, the current in the coil during the launching process was measured using a current probe (Tektronix-TCP2020). The time history of the current with different voltages is shown in Fig. S10 of the ESM. From the results shown, it is clear that the four launching units were approximately equivalent to each other. Therefore, we chose coil 1 to conduct the next analysis.

Using parameters measured from previous experiments, the calculated currents in coil 1 are also plotted in Fig. 4. The calculation process for theoretical current is given in Section S4 of the ESM. Congruence was apparent in most of the launching process. This validates our model. However, there was a certain amount of difference between the theoretical results and the experimental results after about approximately 2.5 ms. After analysis, we found that the main reason for this difference was that we added a freewheel diode in the experiment, which reduced the current oscillation to some extent and caused the experimental results to stabilize after 2.5 ms. In contrast, the existence of the freewheel diode was not considered in the theory and the theoretical result has oscillation after 2.5 ms. The discrepancy shown in the plots can be explained as follows. Firstly, the kinetic energy of the projectile is not considered in the whole model. However, as the projectile is launched, its velocity increases. At some point in the launching process, the influence of projectile velocity cannot be neglected and leads to the discrepancy. Secondly, a freewheel diode is added to the circuit to protect the SCR from the sudden change of coil current. This diode prevents the reversal of the current direction in the coil and helps protect the electrolytic capacitor. In addition, the results for the different voltages are shown in Fig. S11 of the ESM.

4.3 Flight of the projectiles and tethered net

In the sequel, the flight of the projectiles and the tethered net were experimentally investigated. The experimental setup is explained in Section S5 of the ESM.

The tethered net used in the prototypes was made from commercially available fishing nets cut into square pieces, and the elastic modulus was about 1.4 GPa. The four projectiles were then connected to the four corners of the net, as shown in Fig. S12 of the ESM. All projectiles in the experiment were cylindrical threaded pins, with geometric parameters of

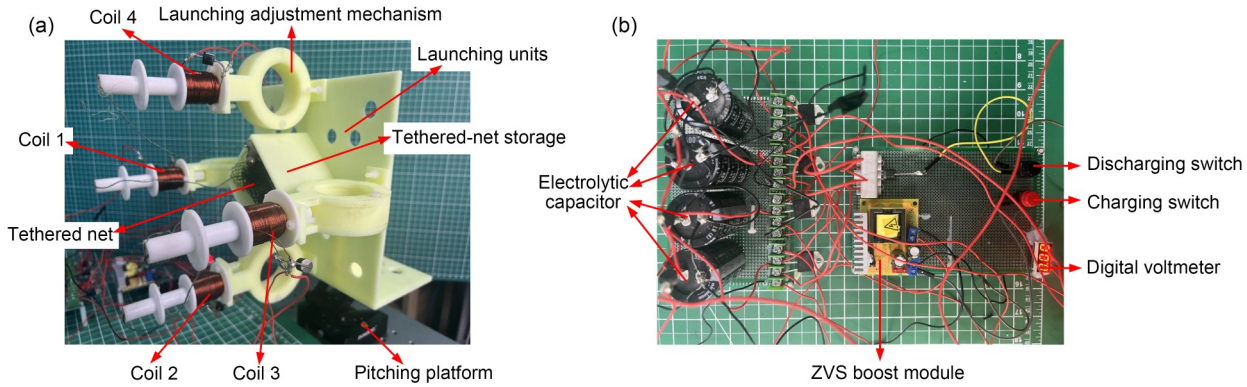

Fig. 3 Mechanical (a) and electrical (b) parts of the launching prototype

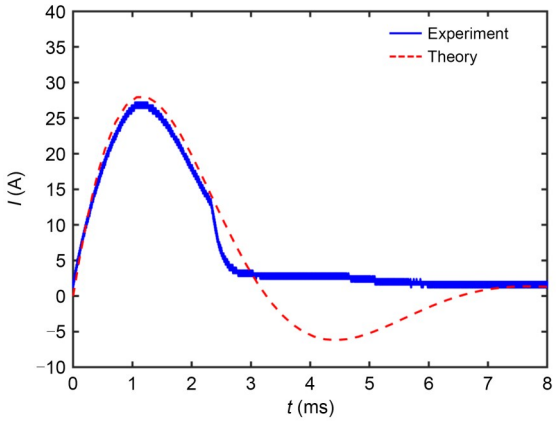

Fig. 4 Time (*t*) history of current (*I*) in the coils during launching with 100 V charged voltage on the capacitor

Φ8 mm×25 mm and a weight of 8 g. However, since the weaving pattern of the net was complex and hard to characterize comprehensively, we adopted some approximate connection patterns for the net and used them to characterize the flight characteristics of the projectiles and the net. In this process, the connection was achieved by high-strength nylon fishing lines with a diameter of 0.5 mm and elastic modulus of 1.9 GPa. The adopted connection patterns are the double-projectile pattern, the square pattern, the cross pattern, and the wiring pattern, as shown in Fig. S12. In the double-projectile pattern, only two projectiles were involved, and they were directly connected by a high-strength nylon fishing line with a length of 60 cm. In the square pattern, the four projectiles were connected by four fishing lines to form a square with a side length of 40 cm. In the cross pattern, two diagonal fishing lines of 60 cm in length were added to the square pattern to connect the two groups of diagonal projectiles. In the wiring pattern, the four projectiles were connected to the four corners of a square net piece of 20 cm side length by fishing lines of 15 cm length. In the experiment, the four projectiles involved were marked with different colors for convenience, and the fishing lines and net were folded into the storage area in an orderly manner.

The obtained flight trajectories of the four projectiles in the wiring pattern were plotted together at different launching angles, as shown in Fig. 5. When the launching angle α=0°, projectile No. 1 landed at 120 ms, projectile No. 2 landed at 110 ms, projectile No. 3 landed at 120 ms, and projectile No. 4 landed at 140 ms. When the launching angle α=10°, projectile No. 1 bounced back at 170 ms and landed at 200 ms, projectile No. 2 landed at 110 ms, projectile No. 3 bounced back at 180 ms and landed at 200 ms, and projectile No. 4 bounced back at 100 ms and landed at 260 ms. When the launching angle α=20°, projectile No. 1 bounced back at 130 ms and landed at 240 ms, projectile No. 2 landed at 140 ms, projectile No. 3 bounced back at 140 ms and landed at 220 ms, and projectile No. 4 bounced back at 130 ms and landed at 260 ms. When the launching angle α=0°, the four projectiles all moved in the positive direction of the *x* axis and there was no rebound phenomenon. When the launching angles α=10° and α=20°, projectiles No. 1, No. 3, and No. 4 bounced back after being maximally separated. However, the rebounding effect was not as apparent as the other three connection patterns because the elastic modulus of the fishing line was greater than that of the net. In addition, there were many meshes in the wire pattern, which affected the rebound effect of the projectile to some extent. Experimental analysis of the other three connection patterns is shown in Section S6 of the ESM.

When the launching angles α=10° and α=20°, because the two coils in the double-projectile patterns were parallel to the horizontal plane, we chose the *x*-*z* coordinate data of the projectile No. 4 from the other

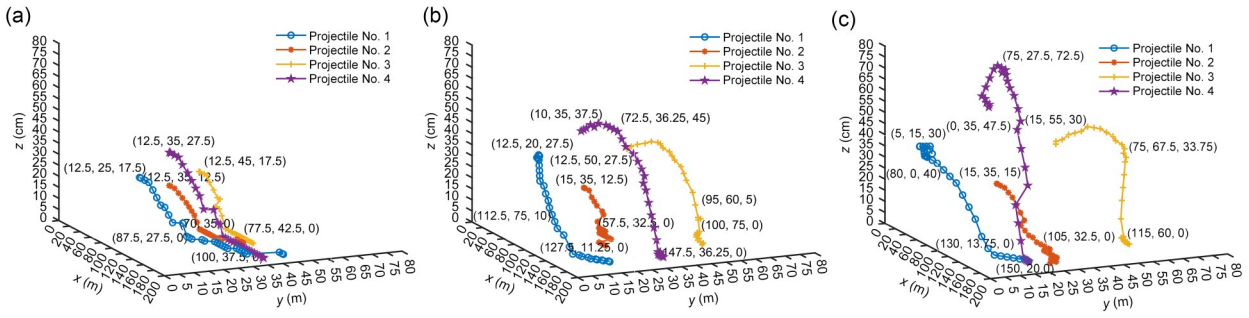

Fig. 5 Flight trajectories of the projectiles in the wire pattern (the initial, bounce-back, and landing coordinates of the projectiles are marked in the figure): (a) α=0°; (b) α=10°; (c) α=20°

three groups of the experiment. Since the initial angles between the projectile No. 4 and the horizontal plane were 20° and 40°, the angles needed to be adjusted to 20° and 40° in the theoretical model. The coordinates are plotted along with their theoretically calculated counterparts in Fig. 6. In the theoretical model, we did not consider the tension of the projectiles, and there were some systematic errors in observing the coordinates of the projectiles. Thus, there is a certain discrepancy between the theoretical and experimental results. This is most obvious in the cross pattern, mainly because there are two diagonal fishing lines connected in the cross pattern. The flight trajectories of the projectiles are divided into two stages. The first stage is before the projectiles are maximally separated. The experimental results for this stage are consistent with the numerical model. The second stage is after the projectiles are maximally separated, and the projectiles bounce back under the tension of the fishing lines. The tension of the diagonal fishing lines on the projectiles is more obvious in the z-axis direction, so the experimental results for this stage are significantly different from the numerical model of the cross pattern. Results for a launching angle of 0° are shown in Section S7 of the ESM.

5 Capture of the object

Finally, we tested the capture performance of the tethered-net launcher. The launcher mentioned above was used in the experiment, as shown in Fig. 3, and the tethered net used for capturing is shown in Fig. S12. A foam cylinder with a diameter of 30 mm and a length of 80 mm was selected as the object. We pushed the target 1700 mm away from the tethered-net launcher and adjusted the launching angle to α=10° and the driving voltage to 150 V. The capture process of the whole experiment is shown in Fig. 7. It can be seen that the capture process took 0.5 s. The net was fully unfolded to the maximum area at 0.2 s and bounced back slightly at 0.3 s. It finally succeeded in capturing the target at 0.5 s. This experimental phenomenon proves that the tethered-net launcher designed by us can successfully capture the object, and demonstrates the feasibility of this method for high-altitude rescue.

It should be noted that as the whole system is designed to capture an object, the unfolding state of the tethered net is not a necessity. As long as the tethered net reaches such a state that it can wrap up the object effectively just before coming into contact with it, capturing can be fulfilled. Whether the tethered net

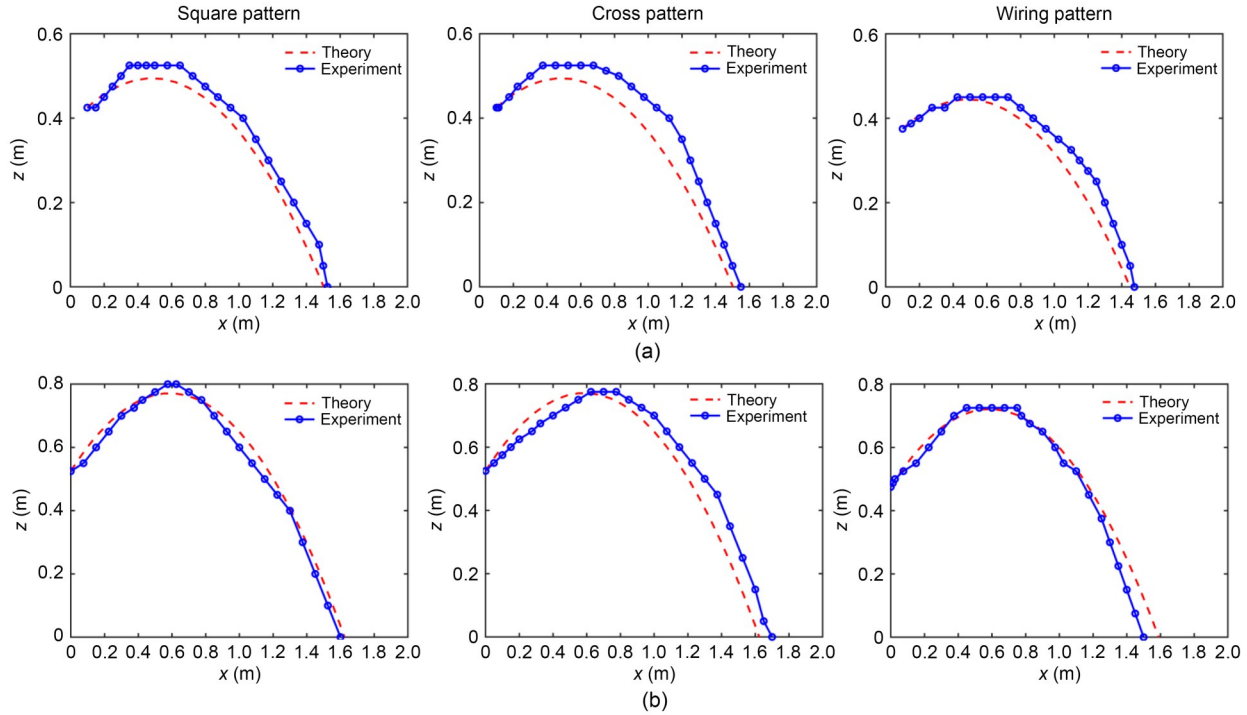

Fig. 6 Theoretical and experimental flight coordinates of the projectiles with different launching angles: (a) α=10°; (b) α=20°

can wrap up the object effectively just before coming into contact with the object is affected by the net size, the launching angle, and the distance of the launching system from the target. The distance of the launching system from the target was considered in the experiment shown in Fig. 7. If the object is close enough to the launching system, the tethered net will not be fully unfolded as it contacts the object. In contrast, if the distance is a little farther, the tethered net will be fully unfolded before it arrives at the object and get into the contracting state when it contacts the object. This is clearly validated by the results shown in Fig. 7. In the experimental settings, the distance between the launching device and the object was around 1.7 m, and the tethered net was fully unfolded before it captured the object. Supposing that the distance was drastically shortened to 0.5 m, it would be very possible that the tethered net would not be fully unfolded when it captured the object. In addition, the size of the tethered net and the launching angle are two important factors to consider. Let us return to Fig. 7, which shows the experiment in which a tethered-net size of 200 mm×200 mm and a launching angle of α=10° were adopted. The unfolding distance of the tethered net was about 850 mm in the experiment. Assuming the tethered net is 100 mm×100 mm or smaller, the unfolding distance will be decreased. Similarly, if the launching angle is adjusted to α=20°, the unfolding distance of the tethered net will be decreased. Therefore, it is not important whether the tethered net is fully unfolded.

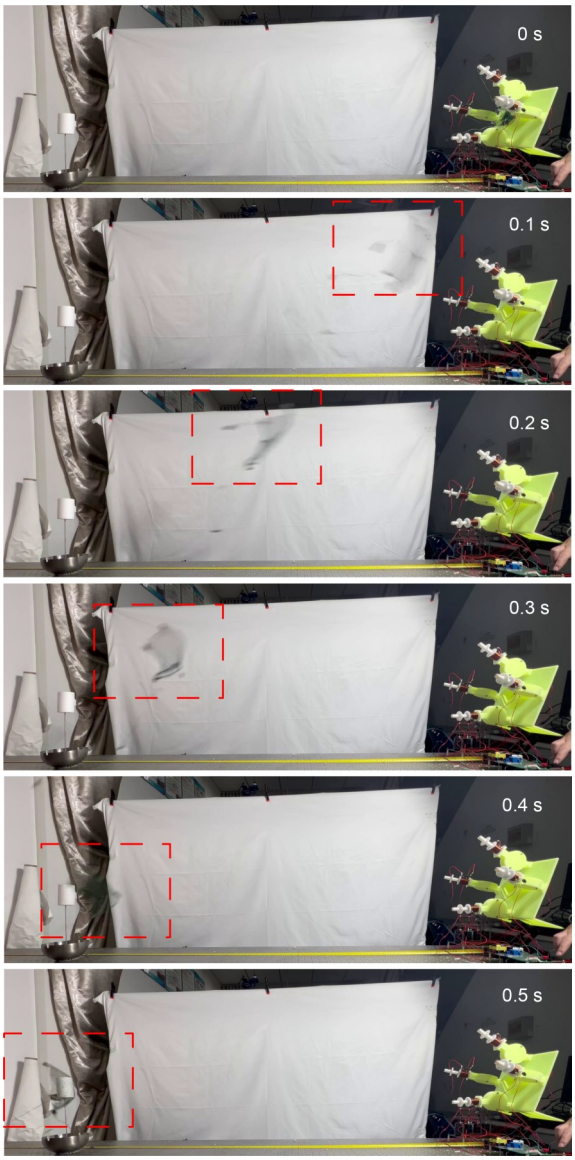

Fig. 7 Positions of the tethered net at different times during flight

6 Conclusions

Aiming to provide an effective and safe method for high-altitude rescue, this paper proposes a tethered-net launcher based on electromagnetic launching units. The launching performance of the units is characterized by measuring and analyzing the exit velocities of the projectiles and the current in the coil. Different projectile connection patterns are considered. Experiments were conducted to explore the flying behaviors of the projectiles and the tethered net with different launching angles. We found that regardless of the connection pattern, with an increase in the launching angle, the time it takes for the tethered net to be maximally unfolded gradually increases. The experimental results are cross-validated with developed theoretical models. A simple capturing experiment using the tethered net was conducted to prove the feasibility of the prototype.

In future research, several directions can be explored. First, optimal control of the launching process is an important goal. With the optimization of the pulsed power supply and the launcher structure, the exit velocity of the projectile should be maximized. Second, the flying performance of the tethered net should be improved. Different ways to store the folded tethered net need to be explored for better launching performance, and the structure of the tethered net

should be optimized for better aerodynamic characteristics. Third, the object-capturing process should be optimized and made smart. Algorithms need to be used to detect, target, and lock the object. Recovering mechanisms should also be included to pull back the tethered net after the object is captured.

This investigation provides a new way to perform high-altitude rescue, based on electromagnetic launching technology. Future investigations and optimizations of the prototypes may prepare them for practical use and application in many rescue situations.

Acknowledgments

This work is supported by the Zhejiang Provincial Natural Science Foundation of China (No. LY22E050013), the China Postdoctoral Science Foundation (No. 2021M690545), and the National Natural Science Foundation of China (No. 51805124).

Author contributions

Zongming ZHU designed the research. Zongming ZHU, Weihao LUO, Zongjing LIN, and Yuzhe KANG conducted the experiment and processed the corresponding data. Zongming ZHU wrote the first draft of the manuscript. Maoying ZHOU, Ban WANG, and Huawei QIN helped to organize the manuscript. Maoying ZHOU revised and edited the final version.

Conflict of interest

The authors have no conflicts of interest to declare that are relevant to the content of this article.

References

Barnes PN, Rhoads GL, Tolliver JC, et al., 2004. Compact, lightweight, superconducting power generators. The 12th Symposium on Electromagnetic Launch Technology, p.158-163. https://doi.org/10.1109/ELT.2004.1398066

Bischof B, 2003. ROGER–Robotic Geostationary Orbit Restorer. The 54th International Astronautical Congress of the International Astronautical Federation, the International Academy of Astronautics, and the International Institute of Space Law. https://doi.org/10.2514/6.IAC-03-IAA.5.2.08

Bresie DA, Andrews JA, 1991. Design of a reluctance accelerator. *IEEE Transactions on Magnetics*, 27(1):623-627. https://doi.org/10.1109/20.101106

Brown MR, Cothran CD, Landreman M, et al., 2002. Energetic particles from three-dimensional magnetic reconnection events in the swarthmore spheromak experiment. *Physics of Plasmas*, 9(5):2077-2084. https://doi.org/10.1063/1.1458589

Chen QQ, Yang LW, Zhang QB, 2009. Dynamic model and simulation of orbital net casting and ground test. *Journal of National University of Defense Technology*, 31(3):16-19 (in Chinese). https://doi.org/10.3969/j.issn.1001-2486.2009.03.004

Chen QQ, Feng ZW, Zhang GB, et al., 2022. Dynamic modeling and simulation of anti-UAV tethered-net capture system. *Journal of National University of Defense Technology*, 44(2):9-15 (in Chinese). https://doi.org/10.11887/j.cn.202202002

Cowan M, Cnare E, Duggin B, et al., 1986. The reconnection gun. *IEEE Transactions on Magnetics*, 22(6):1429-1434. https://doi.org/10.1109/TMAG.1986.1064637

Fair HD, 2009. Advances in electromagnetic launch science and technology and its applications. *IEEE Transactions on Magnetics*, 45(1):225-230. https://doi.org/10.1109/TMAG.2008.2008612

Faraj R, Popławski B, Gabryel D, et al., 2022. Adaptive airbag system for increased evacuation safety. *Engineering Structures*, 270:114853. https://doi.org/10.1016/j.engstruct.2022.114853

Kaye RJ, 2004. Operational requirements and issues for coilgun EM launchers. The 12th Symposium on Electromagnetic Launch Technology, p.59-64. https://doi.org/10.1109/ELT.2004.1398047

Liu YM, Xiong ZM, Chen X, et al., 2022. Simulation and experimental study of the traction and deployment of an interceptive space net wih anti-UAV. *Acta Armamentarii*, 43(9):2048-2057 (in Chinese). https://doi.org/10.12382/bgxb.2022.0258

Ma WM, Lu JY, Liu YQ, 2019. Research progress of electromagnetic launch technology. *IEEE Transactions on Plasma Science*, 47(5):2197-2205. https://doi.org/10.1109/TPS.2019.2902416

McNab IR, 2003. Launch to space with an electromagnetic railgun. *IEEE Transactions on Magnetics*, 39(1):295-304. https://doi.org/10.1109/TMAG.2002.805923

Meinel C, 2007. For love of a gun. *IEEE Spectrum*, 44(7):40-46. https://doi.org/10.1109/MSPEC.2007.376607

Nechitailo NV, Lewis KB, 2006. Critical velocity for rails in hypervelocity launchers. *International Journal of Impact Engineering*, 33(1-12):485-495. https://doi.org/10.1016/j.ijimpeng.2006.09.077

Orbach Y, Oren M, Einat M, 2022. 75 m/s simulation and experiment of two-stage reluctance coilgun. *Journal of Mechanical Science and Technology*, 36(3):1123-1130. https://doi.org/10.1007/s12206-022-0205-8

Sinn T, McRobb M, Wujek A, et al., 2013. Lessons learned from $REXUS_{12}$'S Suaineadh experiment: spinning deployment of a space web in milli gravity. The 21st ESA Symposium on European Rocket and Balloon Programmes and Related Research.

Slade GW, 2005. A simple unified physical model for a reluctance accelerator. *IEEE Transactions on Magnetics*, 41(11):4270-4276. https://doi.org/10.1109/TMAG.2005.856320

Su ZZ, Zhang T, Guo W, et al., 2015. Investigation of armature capture effect on synchronous induction coilgun. *IEEE Transactions on Plasma Science*, 43(5):1215-1219. https://doi.org/10.1109/TPS.2015.2410302

Yu D, Judasz A, Zheng M, et al., 2022. Design and testing of a net-launch device for drone capture. AIAA SCITECH 2022 Forum. https://doi.org/10.2514/6.2022-0273

Electronic supplementary materials

Sections S1–S7, Figs. S1–S12, Tables S1 and S2